Science of the Total Environment 630 (2018) 1381–1393

Contents lists available at ScienceDirect

Science of the Total Environment

journal homepage: www.elsevier.com/locate/scitotenv

Influence of plankton metabolism and mixing depth on CO_2 dynamics in an Amazon floodplain lake

João Henrique F. Amaral [a,b,*], Alberto V. Borges [c], John M. Melack [d], Hugo Sarmento [e], Pedro M. Barbosa [f], Daniele Kasper [a,f], Michaela L. de Melo [e], Daniela De Fex-Wolf [a], Jonismar S. da Silva [a], Bruce R. Forsberg [a]

[a] Coordenação de Dinâmica Ambiental, Laboratório de Ecossistemas Aquáticos, Instituto Nacional de Pesquisas da Amazônia, Manaus, Amazonas, Brazil
[b] Programa de Pós-graduação em Ecologia, Instituto Nacional de Pesquisas da Amazônia, Manaus, Amazonas, Brazil
[c] Chemical Oceanography Unit, University of Liège, Liège, Belgium
[d] Bren School of Environmental Science and Management, University of California, Santa Barbara, CA, USA
[e] Universidade Federal de São Carlos, Departamento de Hidrobiologia, Laboratory of Microbial Processes and Biodiversity, São Carlos, São Paulo, Brazil
[f] Centro de Ciências da Saúde, Universidade Federal do Rio de Janeiro, Rio de Janeiro, Rio de Janeiro, Brazil

HIGHLIGHTS

- Large diel variations on CO_2 dynamics
- Higher plankton metabolism associated with wind mediated mixing.
- Phytoplankton consumption of CO_2 derived from macrophyte decomposition.
- Planktonic respiration is greater in solar exposed chambers.
- CO_2 emissions enhanced during exceptional drought.

GRAPHICAL ABSTRACT

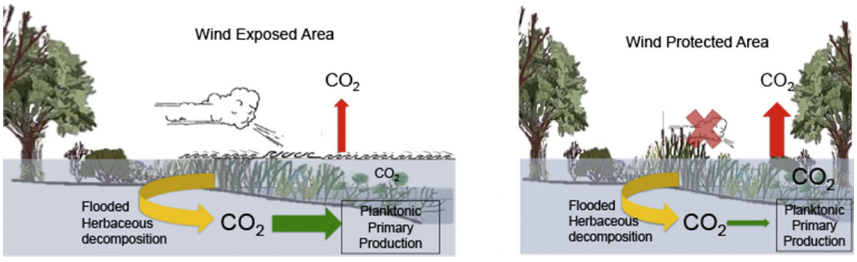

ARTICLE INFO

Article history:
Received 28 December 2017
Received in revised form 27 February 2018
Accepted 27 February 2018
Available online xxxx

Editor: D. Barcelo

Keywords:
Amazon River
Carbon
CO_2 out-gassing
Tropical floodplains
Community respiration
Gross primary production

ABSTRACT

We investigated plankton metabolism and its influence on carbon dioxide (CO_2) dynamics in a central Amazon floodplain lake (Janauacá, 3°23′ S, 60°18′ W) from September 2015 to May 2016, including a period with exceptional drought. We made diel measurements of CO_2 emissions to the atmosphere with floating chambers and depth profiles of temperature and CO_2 partial pressure (pCO_2) at two sites with differing wind exposure and proximity to vegetated habitats. Dissolved oxygen (DO) concentrations were monitored continuously during day and night in clear and dark chambers with autonomous optical sensors to evaluate plankton metabolism. Overnight community respiration (CR), and gross primary production (GPP) rates were higher in clear chambers and positively correlated with chlorophyll-*a* (Chl-*a*). CO_2 air-water fluxes varied over 24-h periods with changes in thermal structure and metabolism. Most net daily CO_2 fluxes during low water and mid-rising water at the wind exposed site were into the lake as a result of high rates of photosynthesis. All other measurements indicated net daily release to the atmosphere. Average GPP rates (6.8 gC m^{-2} d^{-1}) were high compared with other studies in Amazon floodplain lakes. The growth of herbaceous plants on exposed sediment during an exceptional drought led to large carbon inputs when these areas were flooded, enhancing CR, pCO_2, and CO_2 fluxes. During the period when the submerged herbaceous vegetation decayed phytoplankton abundance increased and photosynthetic uptake of CO_2 occurred. While planktonic metabolism was often autotrophic (GPP:CR > 1), CO_2 out-gassing occurred during most periods investigated indicating other inputs of carbon such as sediments or soils and wetland plants.

* Corresponding author at: Programa de Pós-Graduação em Ecologia/INPA-V8, Av. André Araújo 2936, Petrópolis, 69060-001 Manaus, AM, Brazil.
E-mail addresses: jh.amaral@gmail.com (J.H.F. Amaral), alberto.borges@ulg.ac.be (A.V. Borges), john.melack@lifesci.ucsb.edu (J.M. Melack).

https://doi.org/10.1016/j.scitotenv.2018.02.331
0048-9697/

1. Introduction

Aquatic ecosystems on Amazonian floodplains are important components of the regional carbon (C) cycle (Richey et al., 2002; Abril et al., 2013; Melack, 2016; Nagy et al., 2016). A recent estimate (Melack, 2016) indicates that total CO_2 emission from these fluvial wetlands is comparable to that emitted by rivers and streams globally (Raymond et al., 2013) or even higher based on the more conservative estimate of Lauerwald et al. (2015). Large emissions of both CO_2 and methane from Amazon floodplains and their downstream river channels are sustained by organic carbon derived from a variety of floodplain sources (Melack et al., 2004; Engle et al., 2007; Abril et al., 2013). However the temporal dynamics of these contributions at inter-annual, seasonal and diel time-scales is not well understood.

One source of organic C to Amazon floodplain lakes is emergent aquatic vegetation, such as floating herbaceous plants and floodplain forests, that fix CO_2 from the atmosphere and then release dissolved and particulate organic matter and respired CO_2 to the water column (Melack and Engle, 2009; Melack et al., 2009). Organic matter and CO_2 are also derived from phytoplankton and attached algae. Organic C from all these sources is oxidized to CO_2 by planktonic and sedimentary microbial respiration (Waichman, 1996; Engle et al., 2007; Ward et al., 2016). CO_2 is also added to the water column from groundwater and upland streams, benthic communities and other aquatic heterotrophs (Hamilton et al., 1995; Abril et al., 2013). Hence, the excess of dissolved CO_2 in Amazon floodplain lakes results from inputs of CO_2 from several sources with no consensus regarding the relative importance of each and how their contributions vary in time and space (Richey et al., 2002; Johnson et al., 2008; Abril et al., 2013; Borges et al., 2015a; Ward et al., 2016; Melack, 2016). Furthermore, these inputs are expected to vary seasonally in synchrony with the large fluctuation in water level (about 10 m) observed along the Amazon River main channel between high-water and low-water (Junk et al., 1989). This seasonal flood pulse with distinct hydrological phases inundates an extensive floodplain occupied by a mosaic of wetland habitats including alluvial forests, grasslands, and open water environments. During the annual flood cycle, the distribution of flooded habitats and their morphometry (surface area, fetch, depth) vary, leading to changes in thermal stratification and mixing, and in limnological parameters, including chlorophyll *a* (Chl-*a*), dissolved organic carbon (DOC), and dissolved oxygen (DO), that influence C biogeochemistry (Richey et al., 1988; Devol et al., 1988, 1995; Melack and Forsberg, 2001; Abril et al., 2013).

Diel variations in CO_2 or DO can be used to quantify ecosystem metabolic processes. Community respiration (CR) of organic C consumes oxygen, producing CO_2 as a metabolic product, and CO_2 is assimilated into organic C, releasing oxygen, during gross primary production (GPP). GPP and CR can be estimated from changes in CO_2 or DO in dark and light bottles containing lake water during incubations. Alternatively, GPP can be derived independently using stable or radioactive C isotopes (e.g., Steemann Nielsen, 1952; Quay et al., 1995; Bogard and del Giorgio, 2016). The balance or ratio between GPP and CR can be used to infer the autotrophic or heterotrophic nature of an aquatic ecosystem (Odum, 1956; del Giorgio et al., 1999; Cole et al., 2000). Rarely are changes in DO and CO_2 measured together on a diel basis, allowing for the evaluation of aerobic metabolism and its influence on CO_2 dynamics on this time scale. These measurements could also be used to investigate aquatic ecosystems with net autotrophy that have consistent CO_2 out-gassing due to allochthonous and internal CO_2 inputs to the aerobic mixed layer (Dubois et al., 2009; Borges et al., 2014; Bogard and del Giorgio, 2016).

The oxidation of organic C substrates to CO_2 by heterotrophic bacteria in Amazon aquatic ecosystems represents an important CO_2 flux in the regional C balance (Richey et al., 1990; Quay et al., 1992; Waichman, 1996; Engle et al., 2007; Ward et al., 2013). Previous measurements of planktonic CR in Amazon rivers and lakes were made by incubating unfiltered water in the dark for a few hours to days (e.g., Benner et al., 1995; Waichman, 1996; Ward et al., 2013, 2016; Vidal et al., 2015). This practice ignores processes that vary over 24 h-periods, such as algal photosynthesis, that can influence overnight or dark respiration (Sadro et al., 2011, 2014). Different patterns of overnight respiration have been associated with variations in terrestrial inputs, lake productivity and lake residence time (Sadro et al., 2014). These factors might vary in time and space in Amazon floodplain lakes due to the heterogeneity of these systems (Melack and Forsberg, 2001). Furthermore, direct estimates of net planktonic community production (NCP) that include daytime respiration are uncommon in Amazonian aquatic ecosystems (Melack and Forsberg, 2001).

Concentrations of CO_2 in lowland Amazon waters vary over two orders of magnitude and tend to be higher during high water periods and in areas near vegetated habitats (Johnson et al., 2008; Rudorff et al., 2011; Abril et al., 2013; de Rasera et al., 2013; Borges et al., 2015a; Scofield et al., 2016). CO_2 emissions are positively correlated to wind velocity in open waters of lakes and rivers in the Amazon (Alin et al., 2011; Polsenaere et al., 2013; Scofield et al., 2016). Changes in inundated area, vegetated habitats, NCP, wind exposure, fetch, water depth and mixing patterns are also likely to contribute to the observed variations in CO_2 concentrations and fluxes. Variations in CO_2 concentrations and fluxes linked to seasonal floods are likely to increase during extreme floods (Almeida et al., 2017), but the effect of droughts on CO_2 dynamics is unknown although they may be increasing in frequency (Gloor et al., 2013; Marengo and Espinoza, 2016).

Here we use a combination of in situ measurements and enclosed autonomous sensors to investigate seasonal and diel variations in planktonic metabolism (GPP, CR and NCP) and their influence on CO_2 concentrations and emissions in open water habitats of a central Amazon floodplain lake, Lake Janauacá. The large seasonal and spatial variations in the morphometry, hydrology and limnological characteristics encountered in the open waters regions of this lake (Brito et al., 2016) were expected to result in significant variations in wind exposure, lake depth, diel mixing and proximity to emergent vegetation, affecting both CO_2 dynamics and plankton metabolism. CR rates obtained overnight in chambers previously exposed and not exposed to sunlight were compared, and implications for GPP estimates are explored. The combined influence of NCP, aquatic plants, and vertical mixing on CO_2 dynamics in open water floodplain environments are examined together with the implications for the regional C balance. We demonstrate that the plankton community plays a role in regulating CO_2 dynamics, and is capable of absorbing a portion of the dissolved CO_2 resulting from dissolved CO_2 produced during the large scale die-off and decomposition of herbaceous vegetation.

2. Methods

2.1. Study site

Lake Janauacá (3°23′ S, 60°18′ W; altitude 32 m) is located on the right floodplain of the Solimões River, 40 km southeast of Manaus (Fig. 1). It has a local watershed area of 770 km^2 and a floodable area that varies from 23 km^2 at low water to 390 km^2 at high water, with mean annual rainfall of 1980 mm (Pinel et al., 2015). Lake depths vary spatially and seasonally, ranging from in average 1 to 3 m at low water and from 9 to 13 m during high water. The lake is connected to the Solimões River year-round by a 12 km long channel (100–200 m wide). The catchment around the southern part of the lake drains forested and agricultural areas with black and clear water streams of low conductivity (10–30 $\mu S\ cm^{-1}$) and low suspended solid concentrations ($<20\ mg\ L^{-1}$). This part of the lake is dendritic and occupied mostly by open water habitats. An extensive floodplain occupies the northern portion of the lake. The composition of aquatic habitats in this region varies considerably during the year with flooded forests and floating herbaceous macrophytes (*Paspalum repens* P. J. Bergius, *Oryza rufipogon* Griff, *Luziola spruceana* Benth. ex Döll, *Eugenia inundata* D.C.)

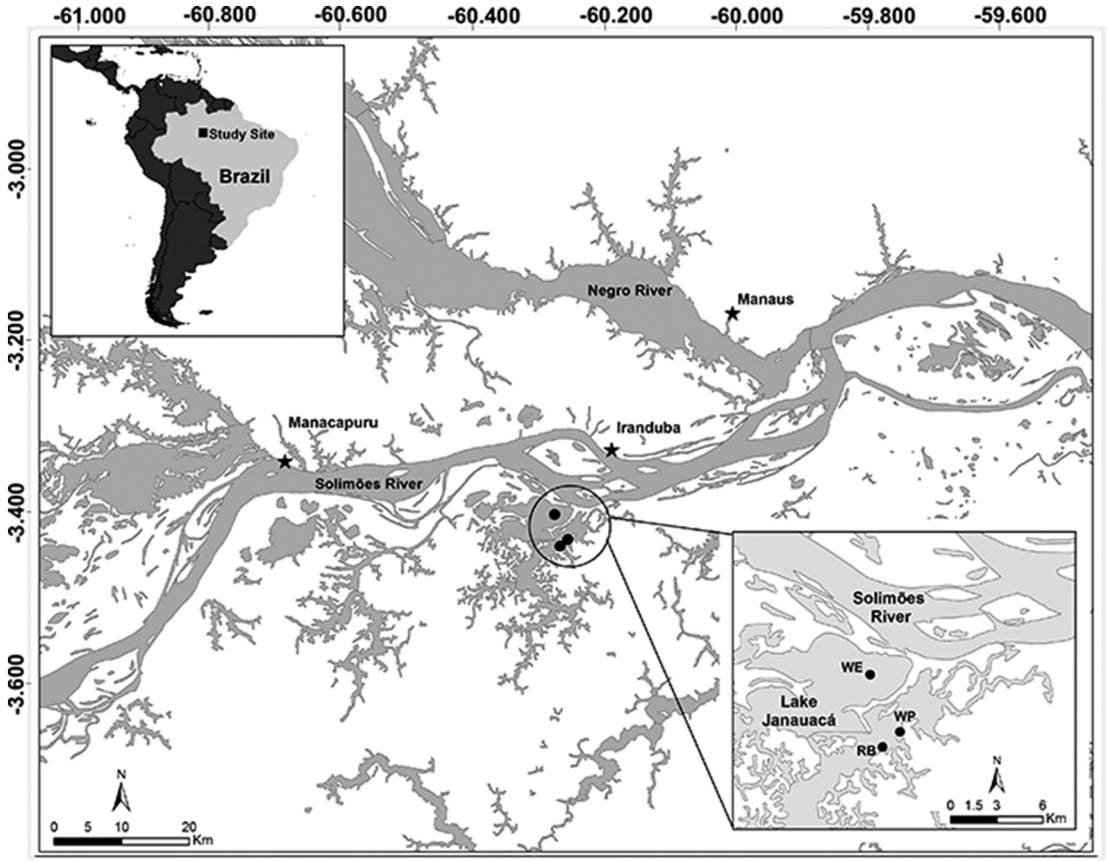

Fig. 1. Map showing the location of the Janauacá floodplain. WE is the location of the wind exposed site and WP is the wind protected site. RB is the research base where the meteorological station was located.

dominating at rising to high water and open water dominating at low water. The lake receives seasonal inputs of Solimões River water containing moderate concentrations of dissolved inorganic nitrogen (12 μmol L^{-1}), soluble reactive phosphorus (0.8 μmol L^{-1}), total nitrogen (23 μmol L^{-1}), total phosphorus (2.4 μmol L^{-1}) and suspended sediments (247 mg L^{-1}) (Forsberg et al., 1988).

2.2. Experimental design

Measurements were made at two open water sites that differed in wind exposure and proximity to vegetated habitats, referred to as the wind exposed (WE) (3°22.6′ S, 60°15.2′ W) and wind protected (WP) (3°24.4′ S, 60°14.8′ W) sites (Fig. 1). The WE site had a fetch of 3 to 6 km and was located 1.5 to 3 km from emergent vegetation, while the WP site had a fetch of 100 m to 1 km and was 30 to 100 m from the nearest emergent vegetation, depending on the season. Depth profiles of carbon dioxide partial pressure (pCO_2) and surface CO_2 emissions were measured at both sites, together with planktonic metabolism (GPP, NCP, CR). Environmental parameters that potentially influenced these variables were also measured including: meteorological variables (wind speed, photosynthetically available radiation (PAR) and air temperature), thermal structure, dissolved organic C (DOC), chlorophyll-*a* (Chl-*a*), colored dissolved organic matter (CDOM) and total suspended sediments (TSS).

Multiple measurements were made during 24-hour periods to investigate the effects of diel variations in metabolism and mixing on CO_2 dynamics, with the exception of May 2016 when only one measurement was made. Measurements were made on six occasions between September 2015 and May 2016, representing different phases of the hydrological cycle: September 2015 (falling water), October 2015 (low water), January 2016 (early rising water), February (mid rising water), April 2016 (late rising water) and May 2016 (early high water). The low water period was atypical and represented an exceptional drought, where the monthly average water levels were below historical values for a similar period due unprecedented warming and lower rainfall throughout much of the Amazon Basin (Jiménez-Muñoz et al., 2016) (Fig. 2).

2.3. Environmental variables and sampling

Each time pCO_2 and CO_2 emissions were measured, depth profiles of conductivity, temperature and dissolved oxygen were obtained. Dissolved oxygen and temperature were measured with a combined temperature/oxygen meter (Yellow Springs Inst. Co., model Pro-ODO, DO accuracy of 0.2 ± 0.1 mg L^{-1}, temperature accuracy ±0.2 °C, resolution 0.1 °C) at 0.5 m intervals. Temperature and conductivity profiles were also measured with a CTD profiler (Castway, Sontek Inst. Co) sampling at 4 Hz with data reported at 0.3 m intervals. Wind speed and direction sensors (Onset, Inc.) were deployed at a height of 2 m on a floating buoy at each site.

Vertical profiles of PAR were determined once during each 24-hour period using an underwater sensor (Licor LI-192 SB). Measurements were made at 0.1 m intervals to the depth where PAR was reduced to 1% of surface irradiance, assumed to represent the depth of the euphotic zone (Z_{eu}). The downwelling extinction coefficient (E_d) was calculated from the slope of a linear regression between the Ln (PAR) and depth. Incident PAR irradiance was measured simultaneously with another sensor (Licor, LI-190). PAR and air temperature were also recorded continuously at a meteorological station (HOBO-Onset) mounted on a floating research station (Fig. 1) about 4 km from the WE site and 1.5 km from the WP site.

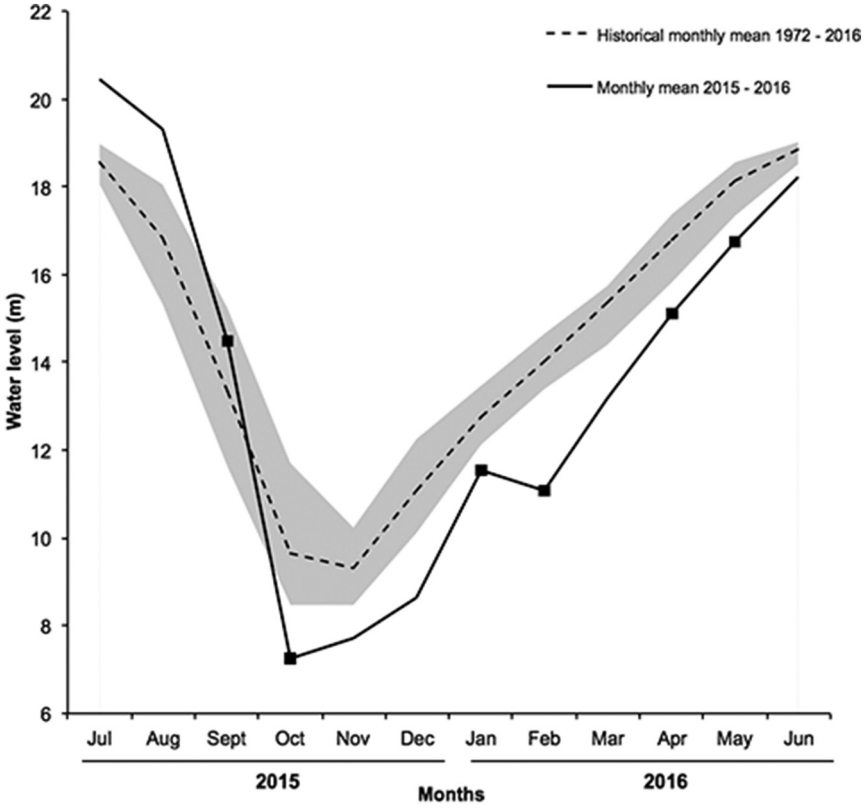

Fig. 2. Historical water levels based on 44 years of daily water level records for the Solimões River at the Manacapuru gauging station. Historical curve (dashed line) represents 44 year monthly means– grey section indicates historic range in monthly means. Solid line indicates observed variation in mean monthly water levels from July of 2015 to June of 2016. Data were downloaded from the Brazilian National Agency of Waters (http://www.snirh.gov.br/hidroweb/).

Water for Chl-*a*, DOC, TSS, and CDOM analyses was collected at both stations at 0.5 m and stored in insulated boxes until processing. Water for Chl-*a* was filtered through glass fiber GF/F filters (Whatman), using a manual vacuum pump in the field, or with an electrical vacuum pump at low pressure (<10 psi) at the floating laboratory. Filters were maintained frozen and in the dark until analysis. Chl-*a* was determined spectrophotometrically, following filter maceration and extraction in 90% acetone, using the trichromatic equations of Strickland and Parsons (1972). TSS was determined by weighing particulates collected on pre-weighed Millipore HA filters (0.45 μm pore size), following the method of Meade et al. (1985). DOC samples were filtered through pre-combusted (450–500 °C for 1 h) glass fiber GF/F filters (Whatman) collected in pre-cleaned (10% HCl wash, deionized water rinse) and pre-combusted (450–500 °C for 1 h) borosilicate vials and then stored at 4 °C until analysis. DOC was determined using a total organic carbon analyzer (TOC-V Shimadzu). Filtered water for spectral analysis was collected in amber borosilicate vials, stored refrigerated (4 °C) in the dark, and then scanned from 180 to 700 nm in a UV-VIS spectrophotometer (Shimadzu UV-VIS 1800) using a 1 cm quartz cuvette and ultra pure water as reference. DOC specific absorbance (a350: DOC mg L^{-1} m^{-1}) and DOC-normalized Chl-*a* (μg mg^{-1}) were used to infer DOC quality (Tranvik and Bertilsson, 2001).

2.4. Metabolic rates

Planktonic NCP, GPP and CR were estimated from changes in DO in water collected from the upper 0.5 m and incubated in situ in three dark and three transparent bottles (2.1 L polystyrene bottles, sealed with silicon stoppers) containing autonomous optical-DO/temperature loggers (PME Inc., MiniDOT®). Lake water for incubations was sampled at the incubation depth with a peristaltic pump (Masterflex, Cole & Parmer Co.) and transferred directly into the incubation bottles, previously cleaned with HCl (10%) and rinsed with distilled water in the laboratory and then rinsed with lake water, together with the logger, in the field. The bottles were overfilled with three times the bottle volumes and closed without bubbles. Dark replicates ($n = 3$) were covered with dark blue tape, then wrapped in aluminum foil and covered with black plastic bags. All transparent ($n = 3$) and dark bottles were incubated at 0.3 m for a minimum of 30 h and a maximum of 72 h. Incubations were done in the open water sampling sites with the exception of April and May when incubations were performed at an open water site close to the floating lab. Profiles of underwater PAR were measured to estimate E_d as described above.

2.4.1. Daily volumetric rates

DO changes (ΔDO) in the incubation bottles were calculated for 10 min intervals and then averaged for 30 min intervals. These average values were used to estimate metabolic rates using values recorded during the first 24 h of incubations. Incubations began at ~6:00 AM (t_0) which corresponded to sunrise. NCP was calculated by multiplying the ΔDO values averaged for the transparent bottles during the daylight period (6:00 h to 18:00 h) by the number of intervals in this period ($n = 24$). We assumed that CR was partially fueled by organic matter produced by phytoplankton during the day and that ΔDO measured in the dark bottles during this period probably underestimate this rate (Sadro et al., 2011, 2014). CR was therefore estimated from the sum of the average 30 min ΔDO values measured in the transparent bottles at night (18:00 h to 6:00 h), after exposition to light during the day, divided by the number of 30 min ΔDO intervals during this period ($n = 24$). We then multiplied this rate by the total number of 30 min intervals in a 24-hour day ($n = 48$), assuming that night and daytime respiration rates were equivalent. This value of daily respiration (CR_{light}) was compared with a parallel estimate of community respiration (CR_{dark}), determined from ΔDO values measured throughout the day in the dark

bottles, to evaluate the importance of photosynthetically derived C during the preceding day for planktonic respiration measured overnight. Differences in how the two estimates were obtained are shown in the Supplementary material (Suppl. mat. Fig. 1). GPP was calculated as the difference between NCP and daily CR_{light} rates, as GPP = NCP − CR_{light}, where CR_{light} is expressed as a negative value.

2.4.2. Daily depth integrated rates

Daily volumetric CR_{light} rates were integrated through the daily average surface mixed layer depth (Z_{mix}) and are expressed as CRL_{zmix}. The value of Z_{mix} was estimated from the DO and temperature profiles made with the YSi probe and with the CTD profiles. We utilized a minimum temperature gradient of 0.2 °C over the depth spacing of the temperature profiles to identify the mixing depth. We calculated a Z_{mix} for each sampling time and averaged all values obtained during 24 h to estimate daily Z_{mix}.

NCP is a light-dependent process and must be integrated with depth to estimate daily integral production. To do this, we first calculated the average PAR in the mixed layer I_{Zmix} (μE m^{-2} s^{-1}) according to Riley (1957),

$$I_{Zmix} = \frac{I_0\left(1-e^{(-Z_{mix}\ E_d)}\right)}{Z_{mix}\ E_d}$$

Z_{mix} is the depth of the average daily mixed layer (m), E_d (m^{-1}) is the downwelling attenuation coefficient, and I_0 (μE m^{-2} s^{-1}) is daily mean incident irradiance. Second, we used an empirical relation (Fig. 3) between volumetric GPP normalized per chlorophyll and the average PAR in the incubated chambers, to estimate the GPP in the mixed layer (GPP_{zmix}) for each sampling site and each sampling occasion. Finally, we subtracted the integrated volumetric respiration rate measured in the light bottles (CRL_{zmix}) from the estimated GPP_{zmix} rate to obtain our integrated NCP rate (NCP_{zmix}). This calculation was necessary because the relationship between NCP normalized to chlorophyll and average incident light was not significant. All rates were converted to C equivalent values using a respiratory quotient of 1. All integrated rates are expressed in g C m^{-2} d^{-1} to be comparable with the CO_2 fluxes, and are expressed with the subscript $Z_{mix,}$. A summary table with all codes and abbreviation is given in Supplementary material (Suppl. mat. Table 1).

2.5. CO_2 dynamics and comparisons with metabolic rates

Levels of pCO_2 were measured with an off-axis integrated cavity output spectrometer (Ultraportable Greenhouse Gas Analyzer - UGGA, Los Gatos Research) connected to a marble-type equilibrator (Frankignoulle et al., 2001), through which flowed lake water was pumped from the upper mixed layer (0.5 m) or from different depths in the case of pCO_2 profiles. The equilibrator consisted of a Plexiglas cylinder (80 cm long) filled with marbles with water entering at the top at a rate of 2–3 L min^{-1} and exiting at the bottom. The UGGA has an internal pump (500 mL min^{-1}) that was connected by an inlet tube at the top of the equilibrator and by an outlet tube at the bottom of the equilibrator allowing the air to circulate through the equilibrator in a closed loop. We used three certified standards (pCO_2 of 1010 and 5000 ppmv, Air Liquid USA and 399 ppmv, White Martins, Manaus, Brazil) to check the factory calibration of the UGGA before each field trip. We used a mixture of argon and nitrogen (White Martins, Manaus, AM, Brazil) passing through fresh soda lime to set the zero, and let the standards flow for at least 3 min through the UGGA. The values from the last minute were averaged and the standard deviation was used to define the precision of the measurements. The average from each standard was plotted to check the linearity of the CO_2 signal, and the slopes and intercepts were compared between calibrations. The precision of the measurements varied between 0.04 and 3.6 ppmv, the accuracy was 104 ± 3.6% for the three standards utilized, and the slopes between calibration events varied from 1.03 to 1.1 with intercepts varying from 1.7 to 33.6.

CO_2 fluxes across the air-water interface were measured using floating chambers connected in a closed loop to the UGGA. Details of the chamber design and deployment method are described in Barbosa et al. (2016). During each flux measurement, CO_2 was measured at 10 s intervals for 10 min. All measurements were made in replicate from a moored boat and no surface currents were observed during measurements. The chambers were exposed to ambient air between measurements to flush the system. Fluxes were calculated from the slope of the partial pressure versus time, which was linear with $r^2 > 0.9$. Fluxes were first calculated in μmol m^{-2} s^{-1} according to the ideal gas law, and then converted to g C m^{-2} d^{-1}. The first minute of each measurement was excluded to allow the system to equilibrate.

To investigate the contribution of NCP to the CO_2 flux, the average daily CO_2 in-gassing or out-gassing flux measured with the chambers was compared to the net CO_2 flux derived from NCP_{zmix}. For this calculation, negative NCP_{zmix} values were considered positive CO_2 fluxes and positive NCP_{zmix} values were considered negative CO_2 fluxes. The differences between these two fluxes was defined as Δ emission (Bogard and del Giorgio, 2016). Negative Δ emission values denoted situations where the net CO_2 flux derived from NCP was greater than the measured CO_2 emission and, thus, sufficient to sustain this emission. When values of Δ emissions were positive, a source of CO_2 in addition to pelagic NCP was required to sustain the observed emission flux.

We used the ratio between GPP_{zmix} and CRL_{zmix} (GPP_{zmix}: CRL_{zmix}) to infer about the planktonic autotrophic or heterotrophic condition at each sampling site during all campaigns. A ratio of GPP_{zmix}: CRL_{zmix} greater than one indicates planktonic autotrophy, while the contrary heterotrophy. A summary flow chart of the methodology is given at the Supplementary material (Suppl. mat. Fig. 2).

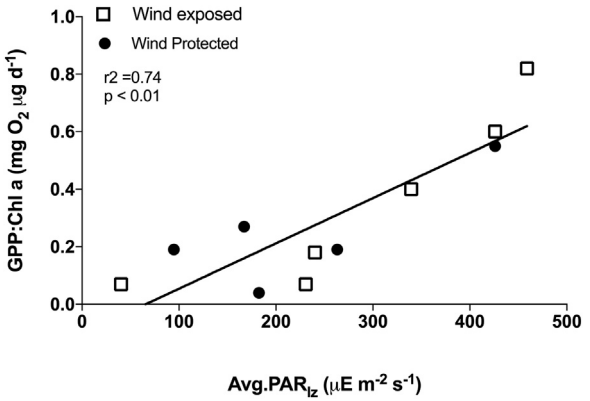

Fig. 3. Volumetric gross planktonic primary production (GPP) normalized by chlorophyll-*a* (Chl-*a*), as a function of average photosynthetically active radiation (PAR) incident on the incubated chambers, measured during incubations in situ. Open squares represent data obtained from the wind exposed site and filled dots from the wind protected site. *p* value was obtained from Pearsons correlation. Volumetric GPP was calculated using respiration rates from the light bottles.

2.6. Statistical analyses

We compared all metabolic rates, pCO_2 and CO_2 fluxes between WP and WE sites with paired *t*-tests, after testing for normality and homoscedasticity. Non-normal variables were transformed before analysis. NCP_{zmix} had negative values and was cubic root transformed. Δ emission also had negative values but remained non-normal after cubic root transformation. In this case, the absolute value of the most negative values was added to all values to create a positive numeric series which was then log transformed. CRL_{zmix}, GPP_{zmix}, Z_{mix}, Chl-*a*, and depth were all log transformed. Pearson correlations were used to determine relationships between DOC characteristics and CR rates, and between GPP: Chl-*a* and PAR. A correlation matrix, including all variables was

used to identify auto-correlated variables. A principal component analysis was then used to define main components and help select variables for use in multiple linear regression models. Δ emissions, pCO_2 and CO_2 fluxes were used as response variables in different regression models. The lowest value of Akaike Information Criterion (AIC) index was used to generate the best regression models. We adopted the 0.05 significance level throughout. Statistical analyses and graphics were done with GraphPad Prism Version 7.01 and with R version 3.3.1 (R Core Team, 2015). Ocean Data View (Schlitzer, 2017) was used to plot the diel CO_2, DO and temperature depth profiles.

3. Results

3.1. Environmental variables

Environmental variables varied considerably between sampling periods and sites. Water depths followed the hydrological cycle (Fig. 2). Average Z_{mix} depths were reduced in periods with water depths <3 m (low water to mid rising water) and greater in periods with depths >5 m (falling water, late rising water and early high water). During the diel cycle, shallow (0.3 m) Z_{mix} values were observed during the day in all periods at the WP site and in the majority of times at the WE site, except during falling water and early rising water when full mixing occurred (Figs. 4 and 5, Suppl. mat. Fig. 4A,; Suppl. mat. Table 2). Values of E_d and Z_{eu} indicated that water was more turbid during low water and early rising water (high E_d and low Z_{eu}), than during falling water (high E_d and low Z_{eu}) (Suppl. mat. Table 2). Average daily incident PAR had a similar range at both sites, but lower values occurred during early rising water and early high water at the WE site and during late rising and early high water at the WP site (Suppl. mat. Table 2) in the days that we performed our 24 h experiments. Wind speeds were higher at the WE (average = 1.9 ± 1.3, range: <±limit (d.l.) to 11.6 m·s^{-1} n = 9125) site compared to the WP site (average = 0.4±, 0.8, range: <d.l. to 5.0 m·s^{-1}, n = 9005) (Paired t-test, $p < 0.01$), where the majority (80%) of the wind speeds were <d.l. of the anemometer of 0.4 m s^{-1} (Suppl. mat. Fig. 3).

Both sites had DOC concentrations close to or >5 mg L^{-1} in periods when decomposition of herbaceous plants occurred: mid rising water and end of rising water. Higher CDOM values were also observed at both sites during these periods. Chl-*a* ranged from 5 to 106 μg L^{-1} at the WE site and from 4 to 27 μg L^{-1} at the WP site. Both sites had high Chl-*a* values during mid rising water (WE = 106 μg L^{-1}; WP = 18 μg L^{-1}) and low water (WE = 54 μg L^{-1}; WP = 27 μg L^{-1}) (Suppl. mat. Table 2).

The amplitude of the diel variation (difference between maximum and minimum) in near-surface DO concentrations was approximately 3 mg L^{-1} at the WP site for all periods investigated. The amplitude of the diel variation of DO at the WE site were greater, and ranged from 7.2 to 13.3 mg L^{-1} during low water (Fig. 4,) and from 4.6 to 11.1 mg L^{-1} during mid rising water (Fig. 5), but only 0.8 mg L^{-1} during early rising water (Suppl. mat. Fig. 4B).

3.2. Metabolic rates

3.2.1. Volumetric metabolic rates

CR_{light} rates (2.5 ± 1.4) were significantly different from CR_{dark} rates (1.7 ± 0.7) (Fig. 6, paired t-test, $p = 0.03$) and, on average, 52% higher, indicating the importance of C inputs from light-mediated processes (e.g., algal photosynthesis) for community respiration. The positive correlation observed between CR_{light}: CR_{dark} and Chl-*a* values at both sites (Fig. 6, $r^2 = 0.47$, $p < 0.05$, $n = 11$) supports this hypothesis. Furthermore, GPP_{zmix} values were, on average, 20% higher when calculated with CR_{light}. We conclude that CR_{light} is the most appropriate parameter to represent plankton CR and hereafter we will present only results for CR_{light} and parameters derived from CR_{light} (such as integrated CR which is CRL_{zmix}) from this point on.

GPP_{light}, NCP and CR_{light} values were highest during low water and lowest during early rising water, with mid to high values recorded during mid-rising water for both sites. NCP rates were 2.8 times higher, on average, at the WE site than at the WP site, varying between −0.7 and 2.4 mg O_2 L^{-1} d^{-1} at the WP site, and from −0.1 to 4.8 mg O_2 L^{-1} d^{-1} at the WE site. GPP_{light} varied between 0.4 and 5.1 mg O_2 L^{-1} d^{-1} at the WP site and between 1.1 and 9.9 mg O_2 L^{-1} d^{-1} at the WE site. GPP_{light} normalized to Chl-*a* increased linearly with average incident PAR ($r^2 = 0.74$, $p < 0.01$, $n = 11$) (Fig. 3).

CR_{light} rates did not differ significantly between sites (paired t-test, $p = 0.058$) but were generally higher at the WE site (Suppl. mat. Table 2). The greatest differences in CR_{light} between sites (2–3 times) were encountered during late rising, low and mid rising water. Similar CR_{light}, and lower values occurred at both sites during early rising and early high water (Suppl. mat. Table 2). We found no statistical relationship between CR rates and DOC concentrations among treatments and sites (Pearson correlation $p > 0.05$), but significant relationship between CR rates and Chl-*a* normalized per DOC (Pearson correlation $p < 0.05$ for CR_{light} both sites, and CR_{dark} at WP site) (Suppl. mat. Fig. 5).

3.2.2. Integrated rates

The largest depth integrated GPP_{zmix} and NCP_{zmix} rates occurred during mid rising water at both sites, followed by the low water period.

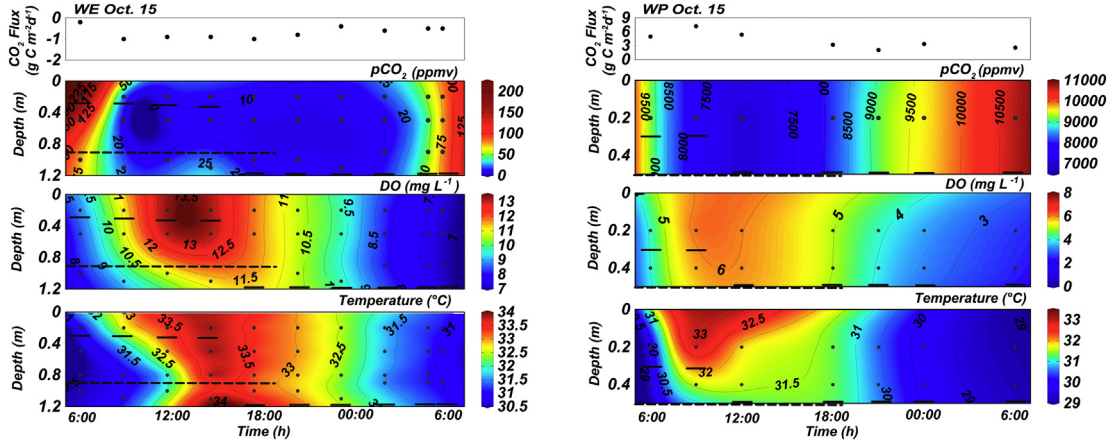

Fig. 4. Twenty-four-hour time-depth diagrams of CO_2 partial pressure (pCO_2), dissolved oxygen (DO) concentrations and temperature, and diel variations in CO_2 flux at the wind exposed (WE) site and wind protected (WP) site during low water period, October 2015. Vertical series of black dots represent measurements made at the indicated time point ± 2 h. Short horizontal solid lines, represents mixed layer depth based on temperature profiles for each sampling occasion. Dashed line represents the depth of the euphotic zone. Note the negative values in Y-axis for CO_2 flux for WE site. Color scales among plots, and depths for each site are different for clarity.

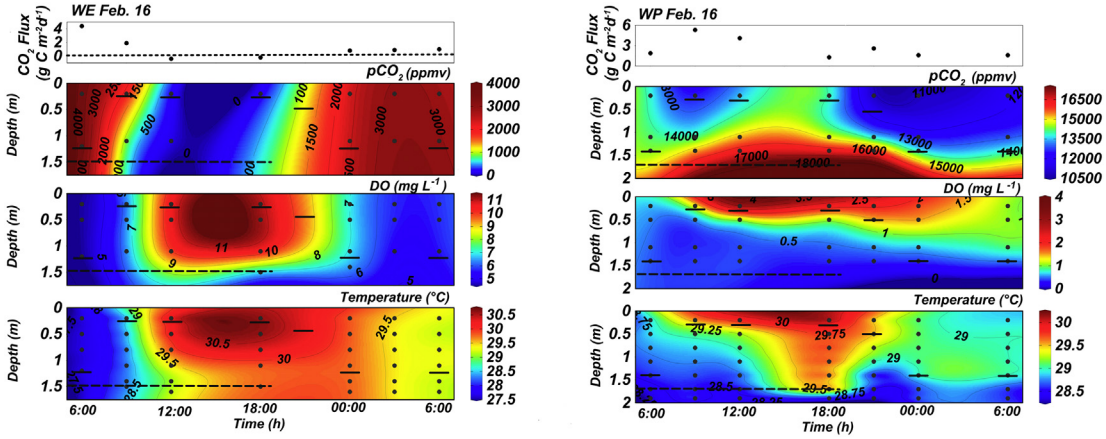

Fig. 5. Twenty-four-hour time-depth diagrams of CO_2 partial pressure (pCO_2), dissolved oxygen (DO) concentrations and temperature, and diel variations in CO_2 flux at the wind exposed site (WE) and wind protected (WP) site during mid-rising water, February 2016. Vertical series of black dots represent measurements made at the indicated time point ± 2 h. Short horizontal solid lines, represents mixed layer depth based on temperature profiles for each sampling occasion. Dashed line represents the depth of the euphotic zone. Dotted line indicates zero value for CO_2 flux, values below this line represent in-gassing fluxes. Color scales differ among plots and depths for each site are different for clarity.

Both integrated rates were much greater (5 to 6 times greater) at the WE site compared to the WP site (Fig. 7, Suppl. mat. Table 2). Higher GPP_{zmix} and NCP_{zmix} rates coincided with periods with high incident PAR and Chl-*a* values, and also with the highest values of the ratio of GPP_{zmix}: CRL_{zmix} (Fig. 7; Suppl. mat. Table 2). Negative NCP_{zmix} values were recorded at the WE site during the other periods when GPP_{zmix}: CRL_{zmix} values were lower than one. The lowest NCP_{zmix} value at the WP site was recorded during late rising water, the only period when GPP_{zmix}: CRL_{zmix} was lower than 1. The lowest GPP_{zmix} at the WE site ($0.80\ g\ C\ m^{-2}\ d^{-1}$) was recorded during early rising water. Similar low values (0.80 and 0.95 $g\ C\ m^{-2}\ d^{-1}$, respectively) were recorded at the WP and WE sites during early high water (Fig. 7).

The highest CRL_{zmix} at the WP site occurred during mid rising water, followed by late rising water, while the lowest rates were recorded at early high water (Fig. 7, Suppl. mat. Table 2). The highest CRL_{zmix} values at the WE site occurred during early high and falling water, while the lowest values were recorded during early rising water.

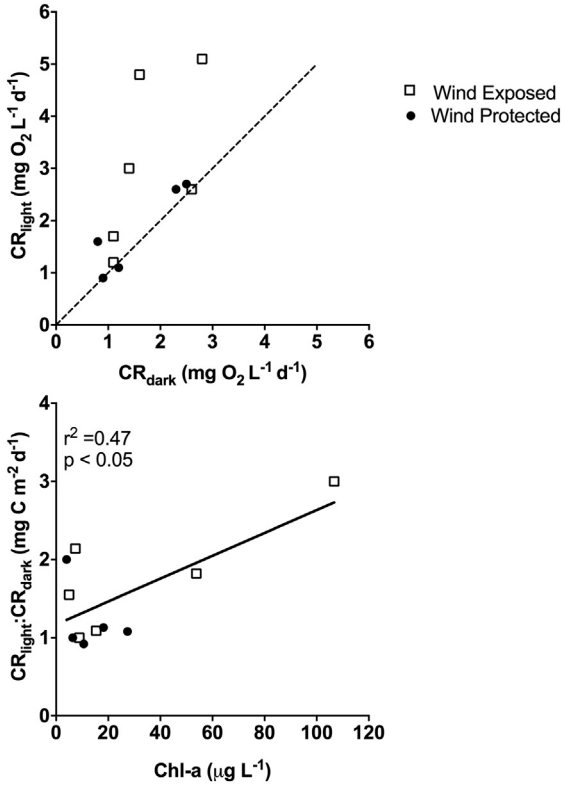

Fig. 6. Comparisons between volumetric community respiration (CR) estimates. The upper graph shows the rates estimated from the transparent bottles (CR_{light}) as a function of the rates estimated in the dark bottles (CR_{dark}). Dashed line represents the 1:1 relation, open squares represent data obtained from the wind exposed site and filled dots from the wind protected site. The bottom graph in the bottom is the ratio between CR_{light} and CR_{dark} as a function of chlorophyll-*a* (Chl-*a*). The *p* value was obtained from Pearson's correlation test and r square by linear regression.

3.3. Metabolic rates and CO_2 dynamics

We used average surface pCO_2 values and CO_2 fluxes obtained during the diel measurements to facilitate comparisons with metabolic rates. Daily average values of pCO_2 were higher at the WP site than at the WE site (paired *t*-test, $p < 0.05$). Daily mean pCO_2 at the WE site was lowest during low water; daily mean pCO_2 at the WP site in the same period was 160 times higher. At this time, we observed decomposing *P. repens* bordering the WP site. Inside the macrophyte debris, we measured an average pCO_2 value of 56,640 µatm (minimum 48,150-maximum 66,290 µatm). The lowest daily average pCO_2 was encountered at the WP site during falling water, while the highest value was recorded during mid rising water. At the WE site, the highest pCO_2 value was recorded during the early rising water. Similar high values were encountered at the WE site during late rising water (Suppl. mat. Table 2). These high pCO_2 values at WE site, coincided with the decay of herbaceous plants that occupied a large portion of the open water region of the lake in early January 2016, when flooding began (Suppl. mat. Fig. 6)

CO_2 fluxes were generally higher at the WE site, except for periods when water was under-saturated in CO_2 (low water and mid rising water) (Figs. 4 and 5; Suppl. mat. Table 2). The highest daily average CO_2 fluxes for the WE and WP sites were recorded during early high water. Among all diel measurements, the highest CO_2 fluxes were recorded during early and late rising water (Suppl. mat. Fig. 4B and C). The lowest average CO_2 fluxes at the WE and WP sites were recorded during low water and falling water, respectively. For the WE site, ingassing fluxes were measured over the day and night during low water, and around noon during mid rising water (Figs. 4 and 5). The lowest CO_2 fluxes at the WP site occurred at the end of rising water and during early rising water (Suppl. mat. Fig. 4B and C).

The difference between measured CO_2 fluxes and NCP_{zmix} or Δ emission was positive for all periods at both sites, except during early high water at the WE site, where the lowest and only negative Δ emission value in the study was recorded (Fig. 8A). The highest Δ emission value was record during the mid-rising water period at the WE site,

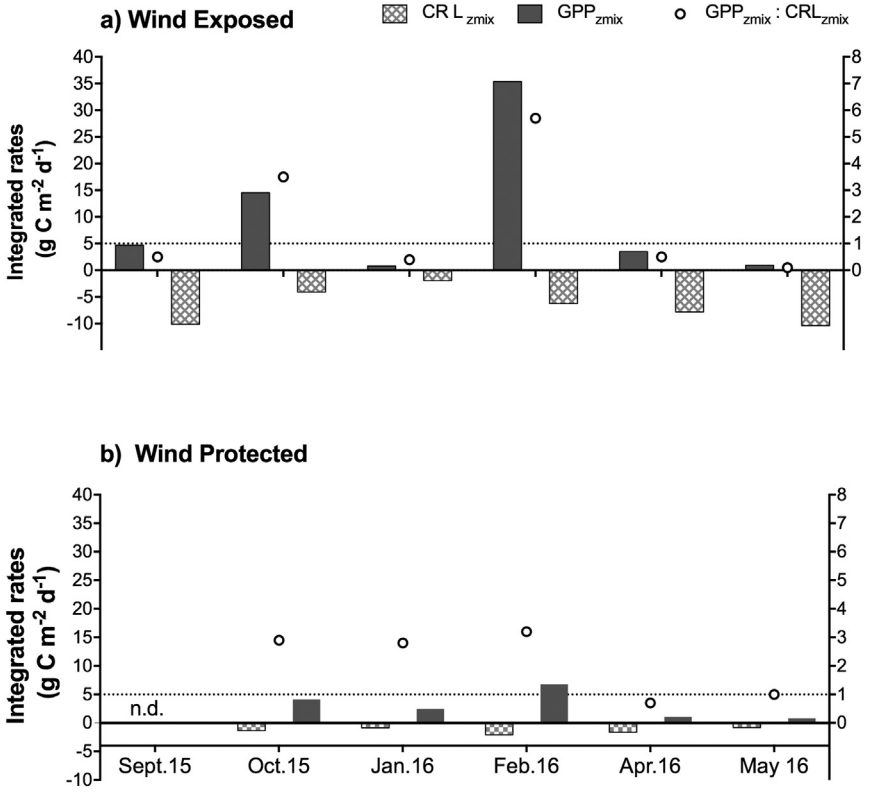

Fig. 7. Variation in integrated metabolic rates over the studied period. Bars represent different metabolic parameters; dark grey bar is integrated gross planktonic production (GPP_{zmix}), light grey bar filled with squares is community respiration estimated from the light bottle (CRL_{zmix}). Open circles represent the ratio between GPP_{zmix} and CRL_{zmix}. Abbreviation (n.d.) for the falling water period (September 2015) represents no data. Dotted line represents a value of 1 for the GPP_{zmix}: CRL_{zmix}ratio.

the same period we registered the highest Δ emission values for the WP site. The lowest Δ emission for the WP site was registered during the late rising water period. Among the positive Δ emission values, five were associated with negative NCP_{zmix} values, GPP_{zmix}: CRL_{zmix} less than one (planktonic heterotrophy) and CO_2 out-gassing (Fig. 8, Suppl. mat. Table 2) and six were associated with positive NCP_{zmix}, GPP_{zmix}: CRL_{zmix} > 1 (planktonic autotrophy) and CO_2 out-gassing (Fig. 8, Suppl. mat. Table 2). The only negative Δ emission value, occurred when NCP_{zmix} was negative and greater in absolute value than the measured CO_2 flux. At this time, the GPP_{zmix}: CRL_{zmix} ratio was exceptionally low and the plankton community generated more than enough CO_2 to sustain the observed out-gassing flux (Fig. 8, Suppl. mat. Table 2).

The PCA with all environmental variables separated sampling sites with different levels of wind exposure (Suppl. mat. Fig. 7). CO_2 dynamics was influenced by environmental variables associated with planktonic metabolism (Chl-*a*) and thermal structure (Z_{mix} and wind speed). Variations in Chl-*a* and Z_{mix} explained 73% of the observed variance in Δ emission while 77% of the variance in pCO_2 was explained by spatial and temporal variations in CO_2 flux and wind speed (multiple linear regressions, Table 1). A single variable, Chl-*a*, explained 54% of the observed variance in CO_2 flux (simple linear regression, Table 1).

3.4. Macrophyte and water level variations

The abundance of floating herbaceous macrophytes varied with changes in water level. Near our sites, *P. repens* was the dominant floating species during 2014 and 2015. Exceptionally low water levels recorded during 2015, caused by a severe drought, led to the mortality of *P. repens* and the emergence of large areas of bottom sediment that were quickly covered with *L. spruceana* and *O.rufipogon* (Suppl. mat. Fig. 6). When water levels started to rise in January and February 2016, these areas were inundated and *L. spruceana* senesced and decomposed. When water levels reached ~5 m (March–April), *O. rufipogon* also senesced and decomposed (Suppl. mat. Fig. 6).

4. Discussion

Our results demonstrate that seasonal variations in environmental factors and in the dynamics of floating herbaceous plants, linked to water level fluctuations, can have a strong influence on concentrations and atmospheric fluxes of CO_2 in the open water areas of Amazonian floodplain lakes. Planktonic metabolism had a strong and direct influence on CO_2 dynamics at low water when vegetated habitats were absent and in periods coinciding with high Chl-*a* values and high PAR. Large increases of pCO_2 and CO_2 fluxes coincided with the death and decomposition of rooted herbaceous plants following inundation. However, most of the CO_2 produced during these events was apparently absorbed by NCP_{zmix} (Fig. 8) and incorporated in plankton community biomass. Variations in wind exposure and, consequently, thermal structure were important factors explaining differences in metabolic rates and CO_2 dynamics between sites in a given season (Table 1, Suppl. mat. Fig. 7). CR measured at night in clear bottles, exposed to sunlight during the day, was higher than that measured in dark bottles through the day (Fig. 6), demonstrating the importance of organic C produced by phytoplankton in fueling plankton CR.

4.1. Metabolic rates and environmental variables

Our depth integrated daily GPP estimates (GPP_{zmix}) were high compared with values reported for other Amazon floodplain lakes. Melack and Forsberg (2001) reported GPP rates between 0.4 and 1.2 g C m^{-2} d^{-1} for Lake Calado, similar to the lowest values found in our study. In a study of plankton metabolism in eight central Amazon floodplain lakes, Forsberg et al. (2017) found daily integral GPP to vary between 0.1 and 11.6 g C m^{-2} d^{-1} with an overall average of

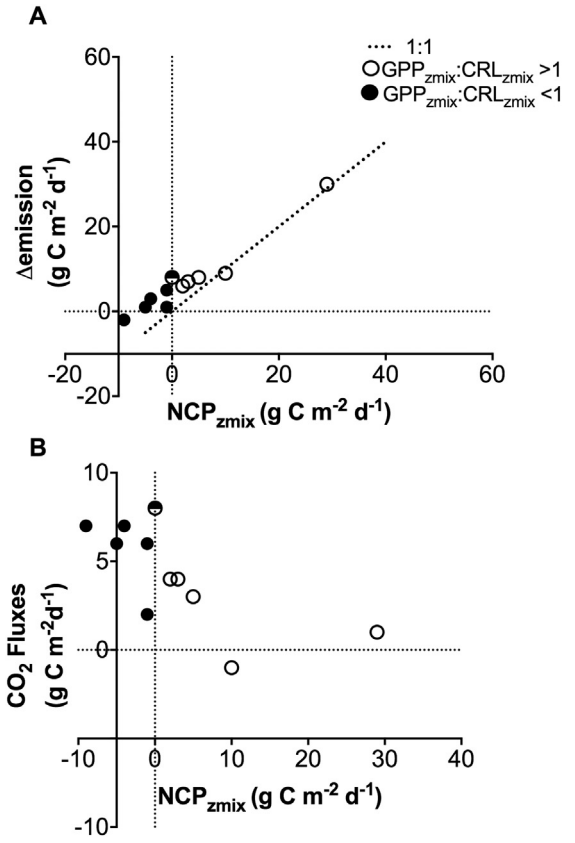

Fig. 8. The Influence of integrated net community production (NCP_{zmix}, g C m^{-2} d^{-1}) on (A) Δ emission (g C m^{-2} d^{-1}): difference between daily average CO_2 fluxes and estimated NCP_{zmix} and (B) the daily average CO_2 flux (g C m^{-2}·d^{-1}). Filled circles represent periods when the ratio between GPP_{zmix} and CRL_{zmix} was lower than one, and open circles represent the opposite. Dashed line in Fig. A represents the 1:1 relation, from which it is possible to interpret the residuals.

2.6 g C m^{-2} d^{-1}, close to the range we found at the WP site (0.8–6.8 g C m^{-2} d^{-1}). The Chl-*a* range that we reported is one order of magnitude higher than the range reported for L. Calado (1–10 μg L^{-1}) (Melack and Forsberg, 2001), but in the range reported by Forsberg et al. (2017) (1.8–142.8 μg L^{-1}). The positive linear relationship we found between Chl-*a* specific GPP and average incident PAR (Fig. 3) indicates that average incident PAR did not exceed the saturation value for photosynthesis, and this relationship could be used to estimate daily integral photosynthesis. The highest GPP_{zmix} values at the WE site coincided with higher Chl-*a* and PAR values (low water and mid rising water), reflecting the causal relationship between these variables (Fig. 3). GPP_{zmix} values at the WE site for other periods were in the range reported by Forsberg et al. (2017).

In comparison to results reported for other open water environments along the Amazon floodplain, our volumetric CR rates (CR_{dark} and CR_{light}) were higher than those based on dark incubations without exposure to natural sunlight during a complete diel cycle. Our lowest CR_{dark} respiration rates (0.8 mg O_2 L^{-1} d^{-1}), were two times higher than the upper range reported in previous studies in other floodplain lakes, and two to four times the average rates in these studies (de Rasera, 2010; Vidal et al., 2015). Our highest CR_{dark} rates for the WP and WE sites were 10 times and 18 times higher, respectively, than the average values cited in these studies. However, our integrated CRD_{zmix} respiration rates (overall average 3 g C m^{-2} d^{-1}, minimum 0.4 and maximum 10.1 g C m^{-2} d^{-1}) were in the range reported in a study of eight central Amazon floodplain lakes, including our study site (Forsberg et al., 2017) (mean: 6.2 g C m^{-2} d^{-1}, minimum 0.16 and maximum 31.3 g C m^{-2} d^{-1}). Compared to a study that compiled CR rates in lakes from different latitudes, our rates were similar or higher than the average rates (Solomon et al., 2013).

4.2. Implications and insights from incubations

That we found higher night-time respiration rates in transparent chambers exposed to natural sunlight during the day (CR_{light}) than in chambers maintained in darkness throughout the incubation CR_{dark} (Fig. 6) is relevant to understanding bacterial metabolism and its relation to substrate quality in Amazonian floodplains. As in other studies in the Amazon basin (Benner et al., 1995; Ellis et al., 2012; Vidal et al., 2015; Ward et al., 2016) and elsewhere (del Giorgio and le Williams, 2005a, 2005b; Solomon et al., 2013), we found little correlation between CR and bulk DOC concentrations. In lakes and other aquatic ecosystems along Amazonian floodplains, the DOC pool is a mixture of refractory organic matter and rapidly cycling labile C (Waichman, 1996; Mayorga et al., 2005). Evidence from isotopic measurements of respired CO_2 and fatty acids indicates that bacterial respiration along the central Amazon floodplain is sustained predominantly by DOC from C4 plants (Quay et al., 1992; Waichman, 1996; Mortillaro et al., 2016). Others, with less direct evidence, suggest that terrestrial C is also important (Ward et al., 2013, 2016). Ward et al. (2016) suggest that there is a priming effect on breakdown of both terrestrially derived C and aquatic plants in the presence of algal C. In addition, they suggest that the reactivity of an organic molecule is dependent on the complex interaction between microbial community composition and environmental factors that might vary on short time scales (minutes to hours). Finally, the availability of DOC for bacteria is dependent on molecular composition and size (Amon and Benner, 1996). The higher CR rates that we measured in transparent chambers suggest that organic matter derived from phytoplankton photosynthesis is an important C source for heterotrophic bacterioplankton. The positive correlations we found between Chl-*a* and CR rates measured in both dark and clear chambers (Fig. 6), as well as DOC-normalized Chl-*a* and CR rates (Suppl. mat. Fig. 5) supports this hypothesis and the conclusions of other studies investigating this relationship in Amazonian rivers (Ellis et al., 2012) and other inland waters (Sadro et al., 2011; Morana et al., 2014). However, phytoplankton also contribute directly to plankton CR and part of increase in CR rates observed in the transparent chambers could be due to the increased metabolic activity of phytoplankton at night as they utilize internal C stores accumulated during the day (Forsberg, 1985). Finally, we assumed that CR measured during the night in a chamber exposed to light during previous day was equal to CR occurring during the day. This may have led to an underestimate of daily CR since there is evidence that CR during the day may be higher than that measured at night (del Giorgio and le Williams, 2005a, 2005b; Pringault et al., 2007).

We report the first measurements of planktonic metabolic rates estimated using continuous records of DO in larger (2.1 L) transparent

Table 1
Multiple regressions coefficients (ß) and intercept (ß0) of the best models for delta emission (Δ emission), carbon dioxide partial pressure (pCO_2), and carbon dioxide fluxes to the atmosphere (CO_2 flux).

	Best model	$\beta_{logChl\text{-}a}$	$\beta_{logzmix}$	$\beta_{CO2\ Flux}$	β_{wind}	β_0	r^2	p	F statistic	AIC
log (x + 3) Δ emission	logChl-*a*, logzmix	0.456	−0.5792			0.4178	0.73	1.9×10^{-3}	14.9(2,8)	−0.355
pCO_2	CO_2 Flux, wind			449.6	−3605.3	8777	0.77	1.1×10^{-3}	17.9 (2,8)	199.53
CO_2 flux	logChl-*a*	−4.929				9.923	0.54	5.5×10^{-3}	13.19 (2,8)	49.14

and dark chambers incubated in Amazon floodplain lakes. The ranges reported for NCP, GPP and CR rates in our study were in agreement with a compilation of metabolic rates estimated from diel free water measurements of DO changes in 25 lakes around the globe, with daily, annual and seasonal estimates of GPP (0.4–25 mg O_2 L^{-1} d^{-1}), NCP (−1–10 mg O_2 L^{-1} d^{-1}) and CR (0.4–20 mg O_2 L^{-1} d^{-1}) (Solomon et al., 2013). The use of continuous records of DO in incubations, in parallel with free water measurements, would improve understanding of lake metabolism in floodplains, allowing investigation of the separate roles of pelagic and littoral metabolism on CO_2 dynamics (Van de Bogert et al., 2007). This approach could help to elucidate spatial differences reported in floodplain lakes and associated with the vegetated areas (Hamilton et al., 1995; Rudorff et al., 2011; Peixoto et al., 2016), although the mass balance computations of the free water measurements require to account for lateral and vertical DO input (Sadro et al., 2014). We chose to perform our incubations in closed chambers to isolate these interferences. Transport of lateral and vertical water masses with contrasting DO concentrations has been observed in an Amazonian floodplain lake (Melack and Fisher, 1983; MacIntyre and Melack, 1995) and in other lakes and wetlands (MacIntyre et al., 2010; Tedford et al., 2014; Poindexter et al., 2016). We recommend that future studies compare metabolic rates derived from free water DO sensors and DO sensors insolated in clear chambers to better understand the participation of plankton metabolism and lateral and vertical advection in the observed diel DO changes.

The higher metabolic rates reported here, when compared to earlier Amazonian studies, may be due to three factors: (1) a larger water volume in the incubations (2.1 L compared to volumes equal or <60 mL in most studies), (2) estimates based on continuous DO records and (3) our in situ incubations resulted in slight mixing within the chambers which would keep plankton in suspension. Large incubation containers are more likely to capture larger plankton organisms which contribute to community respiration (Hopkinson and Smith, 2005). Discrete samples at the beginning and end of incubations can lead to underestimates or overestimations of bacterial respiration rates, compared to rates estimated by continuous DO measurements (Briand et al., 2004).

4.3. Plankton metabolism and its influence on CO_2 dynamics

At the WE site during low water (October 2015), surface waters were under-saturated in CO_2 relative to atmospheric equilibrium during the diel cycle and negative CO_2 fluxes were computed (Fig. 4). DO levels were supersaturated during the same period and inversely correlated with CO_2 throughout the day (Figs. 4 and 9), indicating that the variation in both biogenic gases was tightly controlled by planktonic metabolism. The highest volumetric metabolic rates in the study were recorded for both sites during the low water period. When the water level falls, the connection of floodplains lakes to surrounding emergent vegetation is reduced and pelagic processes, like plankton metabolism, tend to dominate CO_2 dynamics (Melack and Engle, 2009; Abril et al., 2013). This may explain the CO_2 dynamics observed at the WE site at low water. However, decomposing herbaceous plants (*P. repens*) may have also contributed to the high pCO_2 values (daily average 8427 μatm) and high CO_2 fluxes (average 4.1 g C m^{-2} d^{-1}) observed at the WP site during low water.

In February 2016, one month after the decay of debris from *L. spruceana*, surface waters were super-saturated in CO_2 relative to atmospheric equilibrium and positive CO_2 fluxes were observed at the WE site on a daily basis, in parallel with high positive NCP_{zmix}, the highest Chl-*a* in the study, and GPP_{zmix}: CRL_{zmix} ratio greater than one, indicating planktonic autotrophy, but with consistent out-gassing. During the same period, negative CO_2 in gassing fluxes and waters under-saturated in CO_2 were observed around noon, confirming the dominant influence of planktonic metabolism on the diel CO_2 cycle at this time (Fig. 5). NCP_{zmix} was positive and 29 times greater than the daily average CO_2 flux. These results indicate that the majority of the dissolved

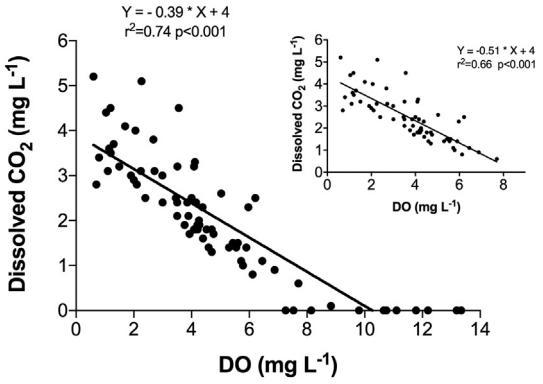

Fig. 9. Dissolved CO_2 concentration as a function of dissolved oxygen (DO). Dots represent all surface records ($n = 75$) over the studied period. The p value was obtained by Person's correlation test and r square by linear regression. Top smaller graph shows the same correlation, but with dissolved CO_2 values greater or equal to 0.6 mg L^{-1}.

CO_2 generated by the decaying plants was taken up by the planktonic community and converted into biomass. What was confirmed by the highest GPP_{zmix} value recorded in our study during the same period. Results from batch incubations with a variety of plant species present in Lake Janauacá, demonstrated the release of large amounts of nutrients during decomposition (Mortillaro et al., 2016). A similar release of nutrients and CO_2 presumably sustained the high levels of NCP_{zmix} observed during this period.

Bogard and del Giorgio (2016), studying 187 boreal lakes, estimated net ecosystem production (NEP) indirectly from deviations in DO saturation under a steady state assumption. They demonstrated that even lakes with net planktonic autotrophic conditions (one third of the studied lakes, with positive Δ emission and NEP values) are likely sources of CO_2 to the atmosphere, due to external inputs of CO_2 and that NEP in planktonic heterotrophic lakes can mirror the external inputs of CO_2. Negative Δ emissions, in this context, denoted situations where the excess of CO_2 produced by NEP was more than sufficient to support the CO_2 emissions, similar to what we observed during the early high water at the WE site, considering only plankton community NCP.

In our study, Δ emission represented the balance between net daily CO_2 production by the plankton community and net daily CO_2 emission to the atmosphere. When Δ emission is zero, all emissions can be accounted for by net planktonic CO_2 production or respiration by the plankton community. When it is negative, net planktonic CO_2 production exceeds emission and when it's positive, other sources of CO_2 are required to account for both emission and net carbon uptake by the plankton community. The relative contributions of NCP_{zmix} and CO_2 emissions to Δ emission can be evaluated by plotting Δ emission against NCP_{zmix} (Fig. 8A). The distribution of points is described by the relationship:

$$\Delta \text{ emission} = NCP_{zmix} + \text{net daily } CO_2 \text{ emission}$$

When net CO_2 emission is zero, all data are expected to fall along a 1:1 line where Δ emission = NCP_{zmix} (Fig. 8A). Positive deviations from this line represent the additional contribution of net daily CO_2 emission to Δ emission. Values of NCP_{zmix} greater or <1 represent situation where plankton metabolism is autotrophic or heterotrophic, respectively. Δ emission was strongly correlated to NCP_{zmix} in this study ($r^2 = 0.94$, $p < 0.001$, $n = 11$), with most points falling close to the 1:1 equivalence line, indicating the dominant influence of plankton metabolism on the CO_2 dynamics of this lake. The equivalence between Δ emission and NCP_{zmix} was strongest when plankton metabolism was autotrophic ($NCP_{zmix} > 1$) and increased with the level of NCP_{zmix}, reaching near equivalence at the highest NCP_{zmix} rates observed at the wind exposed sites during low and mid rising water. Positive deviations for the 1:1 line represented the additional contribution of net CO_2

emission to Δ emission. These deviations tended to be highest and represent a large fraction of Δ emission when plankton metabolism was heterotrophic ($NCP_{zmix} < 1$), although small deviations and net emission fluxes were also observed under most autotrophic conditions, except those associated with the highest positive NCP_{zmix} values (Fig. 8A). The significant regressions obtained for Δ emission against Chl-*a* (positive effect) and Z_{mix} (negative effect) and for net CO_2 emission against Chl-*a* (inverse relationship) (Table 1) indicate the strong influence of these two variables on diel CO_2 dynamics. High levels of Chl-*a* or phytoplankton biomass generally reflected high NCP_{zmix} which was positively related to Δ emission (Fig. 8A) and negatively related to CO_2 emissions (Fig. 8B) in the present study. The effect of Z_{mix} is more complex, as it controls the balance between NCP_{zmix} and CRL_{zmix} in the water column (Sverdrup, 1953). As Z_{mix} increases the proportion of the plankton community present in the euphotic zone declines as does the ratio of GPP_{zmix}: CRL_{zmix} until a critical depth is obtained where this ratio equals 1 and NCP_{zmix} is zero (Sverdrup, 1953). Above this depth NCP_{zmix} is positive and plankton community biomass and below it biomass declines. Since Z_{mix} has a negative relationship with NCP_{zmix} it also tends to have a negative relationship with Δ emission (Fig. 8A).

These results illustrate the central role that plankton metabolism plays in the C dynamics of open water environments along the Amazon floodplain, but also demonstrate the importance of other sources of nutrients, DOC and CO_2 necessary for sustaining high rates of CO_2 outgassing and net plankton community production in these environments (Abril et al., 2013; Borges et al., 2015b; Melack, 2016). These materials could be produced in other wetland environments surrounding these open water areas, such as herbaceous plant beds and floodplain forest, and then transported to these sites by lateral advection or in vegetated habitats covering open water environments at low water that, once flooded, release nutrients, DOC and CO_2 to the overlying waters. The dynamic flow patterns in Amazon floodplain lakes (Lesack and Melack, 1995; Bonnet et al., 2008; Rudorff et al., 2014; Bonnet et al., 2017) may have also influenced our results, either by homogenizing organic C and CO_2 from dominant sources (Waichman, 1996) or by accentuating the relative contribution of contrasting C sources (Moreira-Turcq et al., 2013) at the WE and WP sites in our study.

Among inland waters, tropical rivers, lakes and floodplains account for the majority of the global estimates of CO_2 evasion to the atmosphere (Raymond et al., 2013; Borges et al., 2015b; Melack, 2016). These floodplains have important roles in sustaining CO_2 emissions measured in river channels (Richey et al., 1990; Abril et al., 2013; Borges et al., 2015a, 2015b; Ward et al., 2015, 2016). Melack (2016) noted that about 90% of the lowland Amazon emissions are associated with lakes, floodplains and other wetlands. The diel and seasonal variability in CO_2 fluxes measured in our study emphases the needs for studies on multiple temporal and spatial scales to elucidate uncertainties in regional estimates (Melack, 2016). The differences encountered between measured CO_2 emissions and CO_2 derived from NCP_{zmix} (Δ emission), strengthens the argument that floodplains are important sources of DOC and CO_2 sustaining CO_2 emissions in the lowland Amazon. We observed higher pCO_2 in the wind protected site compared to the wind exposed site. pCO_2 was inversely related to wind velocity and directly related to CO_2 flux in a multiple regression model that explained 77% of pCO_2 variance. CO_2 produced by bacterial respiration and aquatic vegetative root respiration are likely to accumulate in bays that are wind protected, where stability of the water column favors the development of anoxic layers with anaerobic metabolism that contribute to greater CO_2 concentrations (Suppl. mat. Fig. 4A, B and C), as well as CH_4.

Extreme hydrological events are increasingly common in the Amazon region (Marengo and Espinoza, 2016). Two severe droughts were widely reported for the Amazon basin in 2005 and 2010, in association with tropical Atlantic warming and El Niño–Southern Oscillation events (Marengo et al., 2008, 2011; Zeng et al., 2008). Sorribas et al. (2016) analyzed the possible impact of projected climate change scenarios on discharge and precipitation regimes in the Amazon basin, and predicted significant reductions in the extent of inundated areas during low water in the central and lower Amazon. A strong El Niño event in 2015–2016 during our study period resulted in a severe drought (Fig. 2) (Jiménez-Muñoz et al., 2016) causing Lake Janauacá to become almost completely dry at low water (Suppl. mat. Fig. 6), exposing vast areas of lake bottom which were rapidly colonized by herbaceous rooted plants. This resulted in an atypically large input of organic C to the lake when these areas were flooded, and exceptionally high levels of CO_2 concentrations and surface emissions. An increase in the frequency of this type of event could have important consequences for the C balance of lakes along the central Amazon floodplain. The expected increase in CO_2 degassing from floodplain lakes could be balanced by photosynthetic uptake by macrophytes causing no effective change in net CO_2 emission. However, the additional rooted plant biomass might also lead to enhanced carbon burial in floodplain sediments, resulting in the net sequestration of atmospheric CO_2 (Smith et al., 2002; Moreira-Turcq et al., 2004).

5. Conclusions

This study demonstrates that carbon assimilation by phytoplankton can substantially reduce open water CO_2 emissions during periods of large scale mortality and decay of inundated herbaceous plants. The large variations in CO_2 concentrations observed here over 24 h periods and their influence on CO_2 emission have important implications for regional estimates of net C emissions from lakes, which are mostly based on short-term (1–20 min) once daily measurements in open water areas. We conclude that variations in plankton metabolism and wind mediated mixing, linked to spatial and seasonal changes in lake morphometry, have a strong influence on the CO_2 dynamics in Amazon floodplain lakes. Sites with more wind exposure have higher NCP and accumulate less dissolved CO_2 than wind protected areas. We recommend that future studies investigating CO_2 dynamic in lakes consider the influence of variations in plankton metabolism, lake morphometry and stratification patterns at multiple spatial and temporal scales.

Acknowledgements

This work was supported by Ministério da Ciência Tecnologia (CNPq/MCTI); CNPq/LBA-Edital.68/2013, processo 458036/2013-7, CNPq - Universal processo 482004/2012-6. Post-graduate scholarships were provided to JHFA and PMB, by CNPQ and CAPES. JHFA is thankful to the Université de Liège for a research grant (SRDE) and CAPES for the grant "Programa de Doutorado Sanduíche no Exterior -88881.135203/2016-01", JMM received support from NASA (DE-0010620), the US Department of Energy (Contract No. DE-0010620) and a Fulbright fellowship. HS and MLM work was supported FAPESP (Process: 2014/14139-3). AVB is a senior research associate at the Fonds National de la Recherche Scientifique (FNRS). The authors thank for the logistical support of INPA, João B. Rocha for the field support. Ana S. Gomes, Elizandra A. Sampaio and Renata Loureiro for laboratory and field support, Lúcia Silva for offering the floating house as a research base, Ludmila S. Brighenti for discussions regarding the metabolic estimations, Rodrigo Nunes for providing information and discussions related to the macrophytes dynamics at Lake Janauacá, Sally MacIntyre for discussions related to mixing and suggesting the incubations, and Gwenaël Abril for advice on the equilibrator setup.

Appendix A. Supplementary data

Supplementary material includes: (i) a figure showing details of the periods considered in calculations for the different CR estimates, (ii) a flow chart with a summary of the methodology, (iii) figure showing the differences in wind frequency and intensity at the two lake regions investigated in our study, (iv) the representation of diel diagrams of pCO_2, DO, temperature and CO_2 flux for the other periods investigated

in our study at the two regions of the lake that differ in their wind exposure. (v) CR rates as a function of Chl-*a* normalized per DOC for the WE and WP sites, (vi) Sequential Landsat images showing the changes that occurred in the lake during the extreme drough t which affected the herbaceous dynamics, (vii) PCA representation of the environmental variables considered in our study, and a table with all abbreviations used at the manuscript and a table with all data used. Supplementary data to this article can be found online at https://doi.org/10.1016/j.scitotenv.2018.02.331.

References

Abril, G., Martinez, J.-M., Artigas, L.F., Moreira-Turcq, P., Benedetti, M.F., Vidal, L., Meziane, T., Kim, J.-H., Bernardes, M.C., Savoye, N., Deborde, J., Souza, E.L., Albéric, P., Landim de Souza, M.F., Roland, F., 2013. Amazon River carbon dioxide outgassing fuelled by wetlands. Nature 505, 395–398.

Alin, S.R., de Fátima, F.L., Rasera, M., Salimon, C.I., Richey, J.E., Holtgrieve, G.W., Krusche, A.V., Snidvongs, A., 2011. Physical controls on carbon dioxide transfer velocity and flux in low-gradient river systems and implications for regional carbon budgets. J. Geophys. Res. Biogeosci. 116, G01009.

Almeida, R.M., Pacheco, F.S., Barros, N., Rosi, E., Roland, F., 2017. Extreme floods increase CO_2 outgassing from a large Amazonian river: extreme floods increase CO_2 outgassing. Limnol. Oceanogr. 62 (3), 989–999.

Amon, R.M., Benner, R., 1996. Bacterial utilization of different size classes of dissolved organic matter. Limnol. Oceanogr. 41, 41–51.

Barbosa, P.M., Melack, J.M., Farjalla, V.F., Amaral, J.H.F., Scofield, V., Forsberg, B.R., 2016. Diffusive methane fluxes from Negro, Solimões and Madeira rivers and fringing lakes in the Amazon basin. Limnol. Oceanogr. 61, 221–237.

Benner, R., Opsahl, S., Chin-Leo, G., Richey, J.E., Forsberg, B.R., 1995. Bacterial carbon metabolism in the Amazon River system. Limnol. Oceanogr. 40, 1262–1270.

Bogard, M.J., del Giorgio, P.A., 2016. The role of metabolism in modulating CO_2 fluxes in boreal lakes. Glob. Biogeochem. Cycles 30, 1509–1525.

Bonnet, M.-P., Barroux, G., Martinez, J.-M., Seyler, F., Moreira-Turcq, P., Cochonneau, G., Melack, J.M., Resende Boaventura, G., Bourgoin, L.M., León, J.G., 2008. Floodplain hydrology in an Amazon floodplain lake (Lago Grande de Curuaí). J. Hydrol. 349, 18–30.

Bonnet, M.-P., Pinel, S., Garnier, J., Bois, J., Resende Boaventura, G., Seyler, P., Motta Marques, D., 2017. Amazonian floodplain water balance based on modelling and analyses of hydrologic and electrical conductivity data. Hydrol. Process. 31, 1702–1718.

Borges, A.V., Morana, C., Bouillon, S., Servais, P., Descy, J.P., Darchambeau, F., 2014. Carbon cycling of Lake Kivu (East Africa): net autotrophy in the epilimnion and emission of CO_2 to the atmosphere sustained by geogenic inputs. PLoS One 9 (10), e109500.

Borges, A.V., Abril, G., Darchambeau, F., Teodoru, C.R., Deborde, J., Vidal, L.O., Lambert, T., Bouillon, S., 2015a. Divergent biophysical controls of aquatic CO_2 and CH_4 in the World's two largest rivers. Sci. Rep. 5, 15614.

Borges, A.V., Darchambeau, F., Teodoru, C.R., Marwick, T.R., Tamooh, F., Geeraert, N., Omengo, F.O., Guérin, F., Lambert, T., Morana, C., Okuku, E., Bouillon, S., 2015b. Globally significant greenhouse-gas emissions from African inland waters. Nat. Geosci. 8, 637–642.

Briand, E., Pringault, O., Jacquet, S., Torreton, J.P., 2004. The use of oxygen microprobes to measure bacterial respiration for determining bacterioplankton growth efficiency. Limnol. Oceanogr. Methods 2, 406–416.

Brito, B.C., Forsberg, B.R., Kasper, D., Amaral, J.H.F., de Vasconcelos, M.R.R., de Sousa, O.P., Cunha, F.A.G., Bastos, W.R., 2016. The influence of inundation and lake morphometry on the dynamics of mercury in the water and plankton in an Amazon floodplain lake. Hydrobiologia 1–14.

Cole, J.J., Pace, M.L., Carpenter, S.R., Kitchell, J.F., 2000. Persistence of net heterotrophy in lakes during nutrient addition and food web manipulations. Limnol. Oceanogr. 45, 1718–1730.

Devol, A.H., Richey, J.E., Clark, W.A., King, S.L., Martinelli, L.A., 1988. Methane emissions to the troposphere from the Amazon floodplain. J. Geophys. Res.-Atmos. 93, 1583–1592.

Devol, A.H., Forsberg, B.R., Richey, J.E., Pimentel, T.P., 1995. Seasonal variation in chemical distributions in the Amazon (Solimões) River: a multiyear time series. Glob. Biogeochem. Cycles 9, 307–328.

Dubois, K., Carignan, R., Veizer, J., 2009. Can pelagic net heterotrophy account for carbon fluxes from eastern Canadian lakes? Appl. Geochem. 24, 988–998.

Ellis, E.E., Richey, J.E., Aufdenkampe, A.K., Krusche, A.V., Quay, P.D., Salimon, C., da Cunha, H.B., 2012. Factors controlling water-column respiration in rivers of the central and southwestern Amazon Basin. Limnol. Oceanogr. 57, 527–540.

Engle, D.L., Melack, J.M., Doyle, R.D., Fisher, T.R., 2007. High rates of net primary production and turnover of floating grasses on the Amazon floodplain: implications for aquatic respiration and regional CO_2 flux: NPP and turnover of Amazon floating grasses. Glob. Chang. Biol. 14, 369–381.

Forsberg, B.R., 1985. The fate of planktonic primary production. Limnol. Oceanogr. 30, 807–819.

Forsberg, B.R., Devol, A.H., Richey, J.E., Martinelli, L.A., dos Santos, H., 1988. Factors controlling nutrient concentrations in Amazon floodplain lakes. Limnol. Oceanogr. 33, 41–56.

Forsberg, B.R., Melack, J.M., Richey, J.E., Pimentel, T.P., 2017. Regional and seasonal variability in planktonic photosynthesis and planktonic community respiration in Amazon floodplain lakes. Hydrobiologia 800, 187–206.

Frankignoulle, M., Borges, A., Biondo, R., 2001. A new design of equilibrator to monitor carbon dioxide in highly dynamic and turbid environments. Water Res. 35, 1344–1347.

del Giorgio, P.A., le Williams, P.J.B., 2005a. The global significance of respiration in aquatic ecosystems: from single cells to the biosphere. In: del Giorgio, P.A., Williams, P. (Eds.), Respiration in Aquatic Ecosystems. Academic Press, New York, New York, pp. 267–303.

del Giorgio, P.A., le Williams, P.J.B., 2005b. Respiration in Aquatic Ecosystems. New York. Academic Press, New York (326p).

del Giorgio, P.A., Cole, J.J., Caraco, N.F., Peters, R.H., 1999. Linking planktonic biomass and metabolism to net gas fluxes in northern temperate lakes. Ecology 80, 1422–1431.

Gloor, M., Brienen, R.J.W., Galbraith, D., Feldpausch, T.R., Schöngart, J., Guyot, J.-L., Espinoza, J.C., Lloyd, J., Phillips, O.L., 2013. Intensification of the Amazon hydrological cycle over the last two decades. Geophys. Res. Lett. 40, 1729–1733.

Hamilton, S.K., Sippel, S.J., Melack, J.M., 1995. Oxygen depletion and carbon dioxide and methane production in waters of the Pantanal wetland of Brazil. Biogeochemistry 30, 115–141.

Hopkinson, C.S., Smith, E.M., 2005. Estuarine respiration: an overview of benthic, pelagic, and whole system respiration. In: del Giorgio, P.A., Williams, P. (Eds.), Respiration in Aquatic Ecosystems. Academic Press, New York, New York, pp. 122–146.

Jiménez-Muñoz, J.C., Mattar, C., Barichivich, J., Santamaría-Artigas, A., Takahashi, K., Malhi, Y., Sobrino, J.A., van der, Schrier G., 2016. Record-breaking warming and extreme drought in the Amazon rainforest during the course of El Niño 2015–2016. Sci. Rep. 6, 33130.

Johnson, M.S., Lehmann, J., Riha, S.J., Krusche, A.V., Richey, J.E., Ometto, J.P.H.B., Couto, E.G., 2008. CO_2 efflux from Amazonian headwater streams represents a significant fate for deep soil respiration. Geophys. Res. Lett. 35, L17401.

Junk, W.J., Bayley, P.B., Sparks, R.E., 1989. The flood pulse concept in river-floodplain systems. Can. Spec. Publ. Fish. Aquat. Sci. 106, 110–127.

Lauerwald, R., Laruelle, G.G., Hartmann, J., Ciais, P., Regnier, P.A.G., 2015. Spatial patterns in CO_2 evasion from the global river network. Glob. Biogeochem. Cycles 29, 534–554.

Lesack, L.F., Melack, J.M., 1995. Flooding hydrology and mixture dynamics of lake water derived from multiple sources in an Amazon floodplain lake. Water Resour. Res. 31, 329–345.

MacIntyre, S., Melack, J.M., 1995. Vertical and horizontal transport in lakes: linking littoral, benthic, and pelagic habitats. J. N. Am. Benthol. Soc. 14, 599–615.

MacIntyre, S., Jonsson, A., Jansson, M., Aberg, J., Turney, D.E., Miller, S.D., 2010. Buoyancy flux, turbulence, and the gas transfer coefficient in a stratified lake: turbulence and gas evasion in lakes. Geophys. Res. Lett. 37, L24604.

Marengo, J.A., Espinoza, J.C., 2016. Extreme seasonal droughts and floods in Amazonia: causes, trends and impacts. Int. J. Climatol. 36, 1033–1050.

Marengo, J.A., Nobre, C.A., Tomasella, J., Oyama, M.D., Oliveira, G.S., de, Oliveira R., Camargo, H., Alves, L.M., Brown, I.F., 2008. The drought of Amazonia in 2005. J. Clim. 21, 495–516.

Marengo, J.A., Tomasella, J., Alves, L.M., Soares, W.R., Rodriguez, D.A., 2011. The drought of 2010 in the context of historical droughts in the Amazon region. Geophys. Res. Lett. 38, L12703.

Mayorga, E., Aufdenkampe, A.K., Masiello, C.A., Krusche, A.V., Hedges, J.I., Quay, P.D., Richey, J.E., Brown, T.A., 2005. Young organic matter as a source of carbon dioxide outgassing from Amazonian rivers. Nature 436, 538–541.

Meade, R.H., Dunne, T., Richey, J.E., Santos U de, M., Salati, E., 1985. Storage and remobilization of suspended sediment in the lower Amazon River of Brazil. Science 228, 488–490.

Melack, J.M., 2016. Aquatic ecosystems. In: Nagy, L., Forsberg, B.R., Artaxo, P. (Eds.), Interactions between Biosphere, Atmosphere and Human Land Use in the Amazon Basin. Springer Berlin Heidelberg, Berlin, Heidelberg, pp. 119–148.

Melack, J.M., Engle, D., 2009. An organic carbon budget for an Amazon floodplain lake. Verhandlungen des Internationalen Verein Limnologie 30, 1179–1182.

Melack, J.M., Fisher, T.R., 1983. Diel oxygen variations and their ecological implication in Amazon floodplain lakes. Arch. Hydrobiol. 98, 422–442.

Melack, J., Forsberg, B., 2001. Biogeochemistry of Amazon floodplain lakes and associated wetlands. In: ME, McClain, Victoria, R.L., Richey, J.E. (Eds.), The Biogeochemistry of the Amazon basin. Oxford University Press, pp. 235–274.

Melack, J.M., Hess, L.L., Gastil, M., Forsberg, B.R., Hamilton, S.K., Lima, I.B.T., Novo, E.M.L.M., 2004. Regionalization of methane emissions in the Amazon Basin with microwave remote sensing. Glob. Chang. Biol. 10 (5), 530–544.

Melack, J.M., Novo, E.M.L.M., Forsberg, B.R., Piedade, M.T.F., Maurice, L., 2009. Floodplain ecosystem processes. In: Keller, M., Bustamante, M., Gash, J., Silva Dias, P. (Eds.), Geophysical Monograph Series. Vol. 186. American Geophysical Union, Washington, D. C, pp. 525–541.

Morana, C., Sarmento, H., Descy, J.-P., Gasol, J.M., Borges, A., Bouillon, S., Darchambeau, F., 2014. Production of dissolved organic matter by phytoplankton and its uptake by heterotrophic prokaryotes in large tropical lakes. Limnol. Oceanogr. 59, 1364–1375.

Moreira-Turcq, P., Jouanneau, J.M., Turcq, B., Seyler, P., Weber, O., Guyot, J.L., 2004. Carbon sedimentation at Lago Grande de Curuai, a floodplain lake in the low Amazon region: insights into sedimentation rates. Palaeogeogr. Palaeoclimatol. Palaeoecol. 214, 27–40.

Moreira-Turcq, P., Bonnet, M.-P., Amorim, M., Bernardes, M., Lagane, C., Maurice, L., Perez, M., Seyler, P., 2013. Seasonal variability in concentration, composition, age, and fluxes of particulate organic carbon exchanged between the floodplain and Amazon River. Global Biogeochem. Cycles 27, 119–130.

Mortillaro, J.M., Passarelli, C., Abril, G., Hubas, C., Alberic, P., Artigas, L.F., Benedetti, M.F., Thiney, N., Moreira-Turcq, P., Perez, M.A.P., Vidal, L.O., Meziane, T., 2016. The fate of C4 and C3 macrophyte carbon in central Amazon floodplain waters: insights from a batch experiment. Limnologica 59, 90–98.

Nagy, L., Forsberg, B.R., Artaxo, P. (Eds.), 2016. Interactions Between Biosphere, Atmosphere and Human Land Use in the Amazon Basin. Springer Berlin Heidelberg, Berlin, Heidelberg.
Odum, H.T., 1956. Primary production in flowing waters. Limnol. Oceanogr. 1, 102–117.
Peixoto, R.B., Marotta, H., Bastviken, D., Enrich-Prast, A., 2016. Floating aquatic macrophytes can substantially offset open water CO_2 emissions from tropical floodplain lake ecosystems. Ecosystems 19, 724–736.
Pinel, S., Bonnet, M.-P., Santos Da Silva, J., Moreira, D., Calmant, S., Satgé, F., Seyler, F., 2015. Correction of interferometric and vegetation biases in the SRTMGL1 space borne DEM with hydrological conditioning towards improved hydrodynamics modeling in the Amazon Basin. Remote Sens. 7, 16108–16130.
Poindexter, C.M., Baldocchi, D.D., Matthes, J.H., Knox, S.H., Variano, E.A., 2016. The contribution of an overlooked transport process to a wetland's methane emissions. Geophys. Res. Lett. 43, 6276–6284.
Polsenaere, P., Deborde, J., Detandt, G., Vidal, L.O., Pérez, M.A.P., Marieu, V., Abril, G., 2013. Thermal enhancement of gas transfer velocity of CO_2 in an Amazon floodplain lake revealed by eddy covariance measurements. Geophys. Res. Lett. 40, 1734–1740.
Pringault, O., Tassas, V., Rochelle-Newall, E., 2007. Consequences of respiration in the light on the determination of production in pelagic systems. Biogeosciences 4, 105–114.
Quay, P.D., Wilbur, D., Richey, J.E., Hedges, J.I., Devol, A.H., Victoria, R., 1992. Carbon cycling in the Amazon River: implications from the ^{13}C compositions of particles and solutes. Limnol. Oceanogr. 37, 857–871.
Quay, P.D., Wilbur, D., Richey, J.E., Devol, A.H., Benner, R., Forsberg, B.R., 1995. The ^{18}O: ^{16}O of dissolved oxygen in rivers and lakes in the Amazon Basin: determining the ratio of respiration to photosynthesis rates in freshwaters. Limnol. Oceanogr. 40, 718–729.
de Rasera, M.F.F.L., 2010. Determinação dos fluxos de CO_2 e parâmetros físicos envolvidos neste processo em diferentes ambientes fluviais da Amazônia. PhD dissertation. Universidade de São Paulo, Brazil.
de Rasera, M.F.F.L., Krusche, A.V., Richey, J.E., Ballester, M.V.R., Victória, R.L., 2013. Spatial and temporal variability of pCO_2 and CO_2 efflux in seven Amazonian Rivers. Biogeochemistry 116, 241–259.
Raymond, P.A., Hartmann, J., Lauerwald, R., Sobek, S., McDonald, C., Hoover, M., Butman, D., Striegl, R., Mayorga, E., Humborg, C., Kortelainen, P., Dürr, H., Meybeck, M., Ciais, P., Guth, P., 2013. Global carbon dioxide emissions from inland waters. Nature 503, 355–359.
R Development Core Team, 2015. R: A Language and Environment for Statistical Computing. R Foundation for Statistical Computing, Vienna.
Richey, J.E., Devol, A.H., Wofsy, S.C., Victoria, R., Riberio, M.N., 1988. Biogenic gases and the oxidation and reduction of carbon in Amazon River and floodplain waters. Limnol. Oceanogr. 33, 551–561.
Richey, J.E., Hedges, J.I., Devol, A.H., Quay, P.D., Victoria, R., Martinelli, L., Forsberg, B.R., 1990. Biogeochemistry of carbon in the Amazon River. Limnol. Oceanogr. 35, 352–371.
Richey, J.E., Melack, J.M., Aufdenkampe, A.K., Ballester, V.M., Hess, L.L., 2002. Outgassing from Amazonian rivers and wetlands as a large tropical source of atmospheric CO_2. Nature 416, 617–620.
Riley, G.A., 1957. Phytoplankton of the North Central Sargasso Sea, 1950–521. Limnol. Oceanogr. 2 (3), 252–270.
Rudorff, C.M., Melack, J.M., MacIntyre, S., Barbosa, C.C.F., Novo, E.M.L.M., 2011. Seasonal and spatial variability of CO_2 emission from a large floodplain lake in the lower Amazon. J. Geophys. Res. 116, G04007.
Rudorff, C.M., Melack, J.M., Bates, P.D., 2014. Flooding dynamics on the lower Amazon floodplain: seasonal and interannual hydrological variability. Water Resour. Res. 50, 635–649.
Sadro, S., Nelson, C.E., Melack, J.M., 2011. Linking diel patterns in community respiration to bacterioplankton in an oligotrophic high-elevation lake. Limnol. Oceanogr. 56, 540–550.
Sadro, S., Holtgrieve, G.W., Solomon, C.T., Koch, G.R., 2014. Widespread variability in overnight patterns of ecosystem respiration linked to gradients in dissolved organic matter, residence time, and productivity in a global set of lakes. Limnol. Oceanogr. 59, 1666–1678.
Schlitzer, R., 2017. Ocean Data View. http://odv.awi.de.
Scofield, V., Melack, J.M., Barbosa, P.M., Amaral, J.H.F., Forsberg, B.R., Farjalla, V.F., 2016. Carbon dioxide outgassing from Amazonian aquatic ecosystems in the Negro River basin. Biogeochemistry 129, 77–91.
Smith, L.K., Melack, J.M., Hammond, D.E., 2002. Carbon, nitrogen, and phosphorus content and 210Pb-derived burial rates in sediments of an Amazon floodplain lake. Amazoniana 17, 413–436.
Solomon, C.T., Bruesewitz, D.A., Richardson, D.C., Rose, K.C., Van de Bogert, M.C., Hanson, P.C., Kratz, T.K., Larget, B., Adrian, R., Babin, B.L., Chiu, C.Y., Hamilton, D.P., Gaiser, E.E., Hendricks, S., Istvànovics, V., Laas, A., O'Donnell, D.M., Pace, M.L., Ryder, E., Staehr, P.A., Torgersen, T., Vanni, M.J., Weathers, K.C., Zhu, G., 2013. Ecosystem respiration: drivers of daily variability and background respiration in lakes around the globe. Limnol. Oceanogr. 58, 849–866.
Sorribas, M.V., Paiva, R.C.D., Melack, J.M., Bravo, J.M., Jones, C., Carvalho, L., Beighley, E., Forsberg, B., Costa, M.H., 2016. Projections of climate change effects on discharge and inundation in the Amazon basin. Clim. Chang. 136, 555–570.
Steemann Nielsen, E., 1952. The use of radioactive carbon (C^{14}) for measuring organic production in the sea. J. Cons. Int. Explor. Mer 18, 117–140.
Strickland, J.D., Parsons, T.R., 1972. A Practical Handbook of Seawater Analysis. 167. Fisheries Research Board of Canada, Ottawa, Canada (310p).
Sverdrup, H., 1953. On conditions for the vernal blooming of phytoplankton. J. Cons. Int. Explor. Mer 18, 287–295.
Tedford, E.W., MacIntyre, S., Miller, S.D., Czikowsky, M.J., 2014. Similarity scaling of turbulence in a temperate lake during fall cooling. J. Geophys. Res. Oceans 119, 4689–4713.
Tranvik, L.J., Bertilsson, S., 2001. Contrasting effects of solar UV radiation on dissolved organic sources for bacterial growth. Ecol. Lett. 4, 458–463.
Van de Bogert, M.C., Carpenter, S.R., Cole, J.J., Pace, M.L., 2007. Assessing pelagic and benthic metabolism using free water measurements. Limnol. Oceanogr. Methods 5, 145–155.
Vidal, L.O., Abril, G., Artigas, L.F., Melo, M.L., Bernardes, M.C., Lobão, L.M., Reis, M.C., Moreira-Turcq, P., Benedetti, M., Tornisielo, V.L., Roland, F., 2015. Hydrological pulse regulating the bacterial heterotrophic metabolism between Amazonian mainstems and floodplain lakes. Front. Microbiol. 6, 1054.
Waichman, A.V., 1996. Autotrophic carbon sources for heterotrophic bacterioplankton in a floodplain lake of central Amazon. Hydrobiologia 341, 27–36.
Ward, N.D., Keil, R.G., Medeiros, P.M., Brito, D.C., Cunha, A.C., Dittmar, T., Yager, P.L., Krusche, A.V., Richey, J.E., 2013. Degradation of terrestrially derived macromolecules in the Amazon River. Nat. Geosci. 6, 530–533.
Ward, N.D., Krusche, A.V., Sawakuchi, H.O., Brito, D.C., Cunha, A.C., Moura, J.M.S., da Silva, R., Yager, P.L., Keil, R.G., Richey, J.E., 2015. The compositional evolution of dissolved and particulate organic matter along the lower Amazon River—Óbidos to the ocean. Mar. Chem. 177, 244–256.
Ward, N.D., Bianchi, T.S., Sawakuchi, H.O., Gagne-Maynard, W., Cunha, A.C., Brito, D.C., Neu, V., de Matos Valerio, A., da Silva, R., Krusche, A.V., Richey, J.E., Keil, R.G., 2016. The reactivity of plant-derived organic matter and the potential importance of priming effects along the lower Amazon River. J. Geophys. Res. Biogeosci. 121, 1522–1539.
Zeng, N., Yoon, J.-H., Marengo, J.A., Subramaniam, A., Nobre, C.A., Mariotti, A., Neelin, J.D., 2008. Causes and impacts of the 2005 Amazon drought. Environ. Res. Lett. 3, 014002.